



HAL
open science

Extremely Low-Frequency Waves Inside the Diamagnetic Cavity of Comet 67P/Churyumov-Gerasimenko

B. Madsen, C. Wedlund, A. Eriksson, C. Goetz, T. Karlsson, H. Gunell, A. Spicher, Pierre Henri, Xavier Vallieres, W. Miloch

► **To cite this version:**

B. Madsen, C. Wedlund, A. Eriksson, C. Goetz, T. Karlsson, et al.. Extremely Low-Frequency Waves Inside the Diamagnetic Cavity of Comet 67P/Churyumov-Gerasimenko. *Geophysical Research Letters*, 2018, 45 (9), pp.3854 - 3864. 10.1029/2017GL076415 . insu-01897767

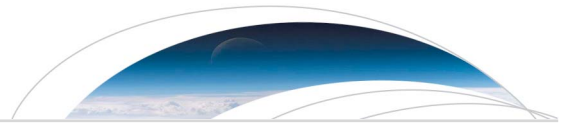
HAL Id: insu-01897767

<https://insu.hal.science/insu-01897767>

Submitted on 24 Oct 2018

HAL is a multi-disciplinary open access archive for the deposit and dissemination of scientific research documents, whether they are published or not. The documents may come from teaching and research institutions in France or abroad, or from public or private research centers.

L'archive ouverte pluridisciplinaire **HAL**, est destinée au dépôt et à la diffusion de documents scientifiques de niveau recherche, publiés ou non, émanant des établissements d'enseignement et de recherche français ou étrangers, des laboratoires publics ou privés.



Geophysical Research Letters

RESEARCH LETTER

10.1029/2017GL076415

Key Points:

- The first continuous low-frequency electric field observations of the diamagnetic cavity of comet 67P/Churyumov-Gerasimenko is here presented
- Observed low-frequency wave activity in the 3- to 8-Hz range is interpreted as ion acoustic waves excitation due to a cavity boundary forcing
- The magnetic and electric fields have similar characteristics while crossing the cavity

Supporting Information:

- Supporting Information S1

Correspondence to:

B. Madsen,
birma@fysik.dtu.dk

Citation:

Madsen, B., Simon Wedlund, C. L., Eriksson, A. I., Goetz, C., Karlsson, T., Gunell, H., et al. (2018). Extremely low-frequency waves inside the diamagnetic cavity of comet 67P/Churyumov-Gerasimenko. *Geophysical Research Letters*, 45, 3854–3864. <https://doi.org/10.1029/2017GL076415>

Received 21 NOV 2017

Accepted 16 APR 2018

Accepted article online 5 MAY 2018

Published online 12 MAY 2018

Extremely Low-Frequency Waves Inside the Diamagnetic Cavity of Comet 67P/Churyumov-Gerasimenko

B. Madsen^{1,2}, C. Simon Wedlund¹, A. Eriksson³, C. Goetz⁴, T. Karlsson⁵, H. Gunell^{6,7}, A. Spicher¹, P. Henri⁸, X. Vallières⁸, and W. J. Miloch¹

¹Department of Physics, University of Oslo, Oslo, Norway, ²Now at Technical University of Denmark, Kongens Lyngby, Denmark, ³Swedish Institute of Space Physics (IRFU), ⁴Institute for Geophysics and Extraterrestrial Physics, Technical University of Braunschweig, ⁵Department of Space and Plasma Physics, School of Electrical Engineering, KTH Royal Institute of Technology, Stockholm, Sweden, ⁶Royal Belgian Institute for Space Aeronomy (BIRA-IASB), Brussels, Belgium, ⁷Department of Physics, Umeå University, Umeå, Sweden, ⁸Laboratoire de Physique et de Chimie de l'Environnement et de l'Espace (LPC2E), Orléans, France

Abstract The European Space Agency/Rosetta mission to comet 67P/Churyumov-Gerasimenko has provided several hundred observations of the cometary diamagnetic cavity induced by the interaction between outgassed cometary particles, cometary ions, and the solar wind magnetic field. Here we present the first electric field measurements of four preperihelion and postperihelion cavity crossings on 28 May 2015 and 17 February 2016, using the dual-probe electric field mode of the Langmuir probe (LAP) instrument of the Rosetta Plasma Consortium. We find that on large scales, variations in the electric field fluctuations capture the cavity and boundary regions observed in the already well-studied magnetic field, suggesting the electric field mode of the LAP instrument as a reliable tool to image cavity crossings. In addition, the LAP electric field mode unravels for the first time extremely low-frequency waves within two cavities. These low-frequency electrostatic waves are likely triggered by lower-hybrid waves observed in the surrounding magnetized plasma.

Plain Language Summary As sunlight heats a comet nucleus, frozen volatile gases sublimate and are ionized and interact with the solar wind and its embedded magnetic field, inducing a dynamical plasma environment around the comet. With the cornerstone European mission Rosetta and its 2 years of near-continuous orbiting of comet 67P/Churyumov-Gerasimenko, the origin, structure, and evolution of this environment are only starting to be unveiled. Exciting are the numerous crossings of the diamagnetic cavity, the innermost plasma region from which the solar wind magnetic field is excluded. Whilst the magnetic field structure of the cavity crossings is well studied, the related electric field activity remains until now unexplored. Studying the electric field with the Langmuir probes onboard Rosetta, we find that whereas the large-scale electric field structure agrees well with the observed magnetic field behavior during cavity crossings, unexpected short-lived low-frequency electric field signals manifest themselves within the cavity. We interpret these as electrostatic waves triggered by a modulating of the cavity boundary caused by observed electrostatic waves at the same frequency in the surrounding magnetized plasma. This unravels a new aspect of the electromagnetic activity in the inner cometary environment, which is crucial for our understanding of the comet-solar wind-induced plasma environment.

1. Introduction

Between August 2014 and September 2016, the European Space Agency (ESA)/Rosetta mission orbited Jupiter-family comet 67P/Churyumov-Gerasimenko (67P) at distances within a few hundred kilometers of the nucleus. Rosetta remained within the inner coma, where cometary ions dominate (Cravens, 1991) and experienced very dynamic plasma regions of varying characteristics (Eriksson et al., 2017; Mandt et al., 2016; Nilsson et al., 2017). These regions are formed as cometary neutral particles, mostly water-group molecules, are outgassed from the cometary nucleus, ionized by photons and electron impact, and interact with the solar wind plasma and its embedded magnetic field (Cravens, 1989; Simon Wedlund et al., 2017). Between perihelion and a heliocentric distance of 2.4 astronomical units (AU), the increased outgassing of comet 67P led to the lasting formation of a magnetic field-free (diamagnetic) cavity in the innermost part of the cometary coma

(Goetz, Koenders, Richter, et al., 2016). Within this region, cometary ions and neutrals are coupled. The existence of the diamagnetic cavity at 67P was predicted by models (Hansen et al., 2007) but its electromagnetic characteristics remained experimentally unexplored until Rosetta's in situ observations.

We report the first continuous electric field observation of the cometary diamagnetic cavity at 67P by the Langmuir probe (LAP) instrument (Eriksson et al., 2007) as part of the Rosetta Plasma Consortium (RPC), a suite of five instruments on Rosetta observing the cometary plasma environment (Carr et al., 2007).

The cometary diamagnetic cavity is confined by the contact surface usually attributed to the balance between the outward ion-neutral friction force and the inward solar wind magnetic pressure gradient and tension forces (Cravens, 1986; Ip & Axford, 1987; Timar et al., 2017). Predicted prior to any cometary missions (Biermann et al., 1967), this region was first observed in situ during the Giotto flyby of comet 1P/Halley (Neubauer et al., 1986).

Exploring the diamagnetic cavity, its formation, growth, and characteristics in the case of a low-outgassing comet such as 67P is an important goal of the RPC (Glassmeier, 2017; Hajra et al., 2018; Nemeth et al., 2016). A major result of the mission includes more than 650 magnetic field detections of comet 67P's diamagnetic cavity (Goetz, Koenders, Hansen, et al., 2016). Observations of these regions typically lasted 30 s to tens of minutes due to the fast movement of the structures over the slow-moving spacecraft. The magnetic field-free cavity observations were typically preceded by a relatively long inbound boundary characterized by a gradual decrease in the magnetic field magnitude and succeeded by short outbound boundary regions within which the magnetic field rapidly regained its magnitude (Goetz, Koenders, Hansen, et al., 2016). The electric field characteristics remain, however, mainly unexplored.

The existence of electromagnetic waves at the cavity boundary is expected due to currents and large density gradients forming there (Israelevich et al., 2003). This current may drive lower-hybrid drift instabilities (LHDI) as well as two-beam instabilities that can excite waves in the lower-hybrid (LH) and ion acoustic wave (IAW) frequency ranges, which in turn can heat up and accelerate the plasma (e.g., Bingham et al., 1991).

Outside of 67P's cavity, RPC instruments have recorded a wealth of electromagnetic fluctuations and waves triggered by instabilities: low-frequency electromagnetic waves attributed to modified ion-Weibel instabilities in the 40-mHz range (Meier et al., 2016; Richter et al., 2015), LH waves around a few Hz due to plasma density gradients (André et al., 2017; Karlsson et al., 2017), and IAW at frequencies > 200 Hz, possibly excited by current-driven instabilities (Gunell, Nilsson, et al., 2017).

Inside 67P's cavity, Gunell, Goetz, et al. (2017) recently showed evidence of dampened current-driven IAW near 200 Hz, using the current measured by LAP on 3 August 2015. Unfortunately, with 85.3-ms samples taken every 160 s, a continuous observation of the electrostatic wave activity of the cavity was impossible. Another way to measure electric fields is to operate the LAP instrument in electric field mode using two probes for detection of low-frequency activity (Eriksson et al., 2007). Because this mode could only be used during favorable pointing conditions with simultaneous solar illumination of both probes (Karlsson et al., 2017), we found only four diamagnetic cavity crossings coinciding with electric field measurements.

In this work, we investigate the low-frequency electric field signatures of four cavity crossings observed on 28 May 2015 and 17 February 2016 and reveal extremely low-frequency electrostatic wave activity within the cavity. These observations add essential information about the electromagnetic activity in and around the diamagnetic cavity towards the goal of characterizing the comet-solar wind interaction region.

2. Instrumentation

The instruments of the RPC (Carr et al., 2007) provide information about the structure and evolution of the comet-solar wind interaction region at comet 67P (Glassmeier, 2017). The LAP instrument has as its sensor elements two spherical Langmuir probes, LAP1 and LAP2, mounted at the ends of a 2.24- and a 1.62-m-long booms (Eriksson et al., 2007). By measuring the floating potential differences V_1 and V_2 between the probes and the spacecraft body, the electric field between the probes can be estimated as the difference in potential ($V_2 - V_1$) divided by the probe separation distance (Karlsson et al., 2017). For the studied events, the LAP electric field mode continuously samples at 57.8 samples per second with short data gaps (about 1 s) every 32 s. Following Karlsson et al. (2017), any signal below 1 Hz is neglected due to spurious effects in the lowest frequency range, for instance, introduced by asymmetries in the probe positions relative to the spacecraft body.

Depending on the orientation of the spacecraft, LAP1 and LAP2 might be shadowed by the solar panels and the high-gain antenna, respectively. While shadowing from the solar panels can be calculated from the spacecraft pointing direction (Johansson et al., 2017), the high-gain antenna complicates the accurate determination of LAP2 shadowing. Throughout the 28 May 2015 events, both probes were sunlit. However, data show that LAP2 was either partially or completely shadowed during the 17 February 2016 events. If illumination conditions are constant and if the probes couple sufficiently well to the plasma, changes in the probe potentials may, additionally, give information about changes in the spacecraft potential, and hence, variations in the electron plasma density and temperature when the photoemission current to the spacecraft remains unchanged (Odelstad et al., 2015).

To determine the timings of the cavity crossings, observations by the RPC fluxgate magnetometer (MAG, Glassmeier et al., 2007) are included. The MAG sensors are mounted on the same boom as LAP2 and measure the three-component magnetic field. The components are given in the comet-centered solar equatorial frame, with the x -axis pointing towards the Sun, and the z -axis parallel to the part of the Sun's rotational axis that is perpendicular to the x -axis. The y -axis completes a right-handed system (Broiles et al., 2015). The magnetic fields have been calibrated according to the method described in Goetz, Koenders, Hansen, et al. (2016), and the maximal temporal resolution is 20 vectors per second.

The RPC Mutual Impedance Probe (MIP; Trotignon et al., 2007) measures the electric impedance between a set of transmitters and receivers. Under certain conditions, spectral characteristics of the impedance can be used to estimate the plasma frequency and thus the local electron density, with a temporal resolution of 2.5 to 32 s (Henri et al., 2017). The spectral characteristics of the mutual impedance did not allow for retrieving the electron density during the 28 May 2015 events, but the electron density could be derived for the 17 February 2016 events.

3. Observations

Out of the at least 665 MAG diamagnetic cavity detections at comet 67P (Goetz, Koenders, Hansen, et al., 2016), only two dates coincide with LAP electric field observations, due to the rare operation of the electric field mode. The first (second) was at heliocentric and cometocentric distances of 1.54 AU (2.38 AU) and 270 km (42 km), respectively, on 28 May 2015 (17 February 2016) in preperihelion (postperihelion) conditions. On both days, Rosetta crossed the cavity twice.

In this section, we present the one-dimensional electric field of the four crossings. For the May 2015 events (crossings A and B), we additionally study the electric field spectra. However, during the February 2016 events (crossings C and D), a partial shadowing of LAP2 resulted in artificial narrow band frequency emissions, making the interpretation of the corresponding electric field spectra difficult. A spectral analysis of the electric field during crossings C and D is therefore excluded from this work.

Figures 1a–1c, 2a–2c, and 3a–3c show overviews of the magnetic fields, electric fields, and probe potentials during the crossings (see supporting information for a schematic of the transition). The cavity crossings are characterized by relatively small fluctuations in the magnetic field components. The timings of the transitions into and out of the cavities are defined following the convention in Goetz, Koenders, Hansen, et al. (2016) and given in Table 1. The magnetic field components are cavity-calibrated by subtracting the means of each component within the cavity. The calibrations for crossings A and B vary slightly from one another due to changes in the local plasma environment.

Crossings B, C, and D show magnetic field signatures typical of diamagnetic cavity crossings at comet 67P (Goetz, Koenders, Hansen, et al., 2016): a long inbound transition region, with a gradual decrease in all three magnetic field components, compared to a sharp outbound transition, where the fluctuation levels of the components rapidly increase. The difference in temporal extent of the inbound and outbound transition layers of crossing A is less pronounced.

The electric fields in Figures 1b, 2b, and 3b are detrended by subtracting a 1-s moving average to filter out low-frequency components. The intervals of strongly reduced electric field activity coincide well with the cavity timings determined by the magnetic field. Following the behavior of the magnetic field, the electric field fluctuation levels gradually decrease throughout the inbound transition layers, and for crossings B, C, and D, the outbound boundaries are subject to sharp increases in the activity. For all events, the outbound transitions are associated with probe potential increases (Figures 1c, 2c, and 3c), mainly reflecting changes in the electron

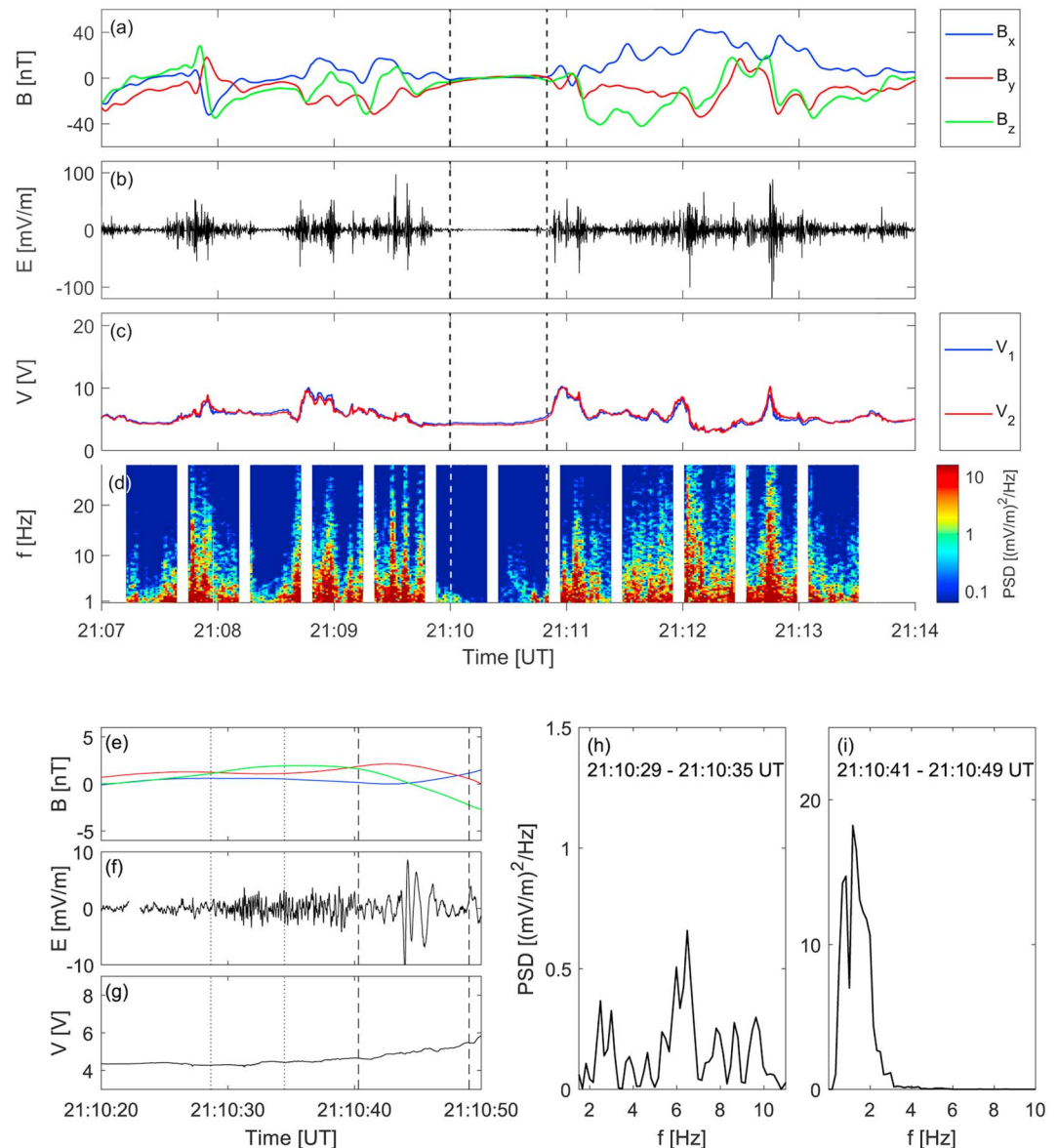


Figure 1. Signatures at crossing A (21:10:00–21:10:50 UT) on 28 May 2015. (a) Cavity-calibrated MAG magnetic field components in comet-centered solar equatorial coordinates. (b) Detrended Langmuir probe (LAP) electric field measurement. (c) LAP probe potentials. (d) Electric field Fourier spectrogram. The vertical dashed lines mark the timings in and out of the cavity. (e)–(g) Magnetic field, electric field, and averaged probe potentials inside the cavity. (h)–(i) Power spectral densities (PSD) over intervals limited by the vertical dotted and dashed lines in panels e–g.

density and/or temperature. This suggests asymmetries in the electron profiles at the inbound and outbound transitions, as confirmed, for the February events, by the MIP-derived electron density (Figure 3d).

3.1. Transient Electric Field Activity Inside the Diamagnetic Cavity

Figures 1d and 2d show electric field Fourier spectrograms over crossings A and B. The spectrograms are constructed from fast Fourier transform power spectral densities (PSDs) computed over 4-s Hanning-windowed subintervals of the detrended continuous electric fields (Welch, 1967), giving a frequency resolution of 0.25 Hz. Other levels of detrending and windowing, as well as a Morlet wavelet analysis (Morlet et al., 1982; Torrence & Compo, 1998) of the signals (not shown), show features similar to those seen in the Fourier spectrograms, supporting the reliability of observed features. The spectrograms reveal temporally varying low-frequency electric field activity below 10 Hz within the cavity; between 21:10:29 UT and 21:10:49 UT for crossing A and between 21:52:13 UT and 21:53:20 UT for crossing B. Figures 1e–i and 2e–i focus on short

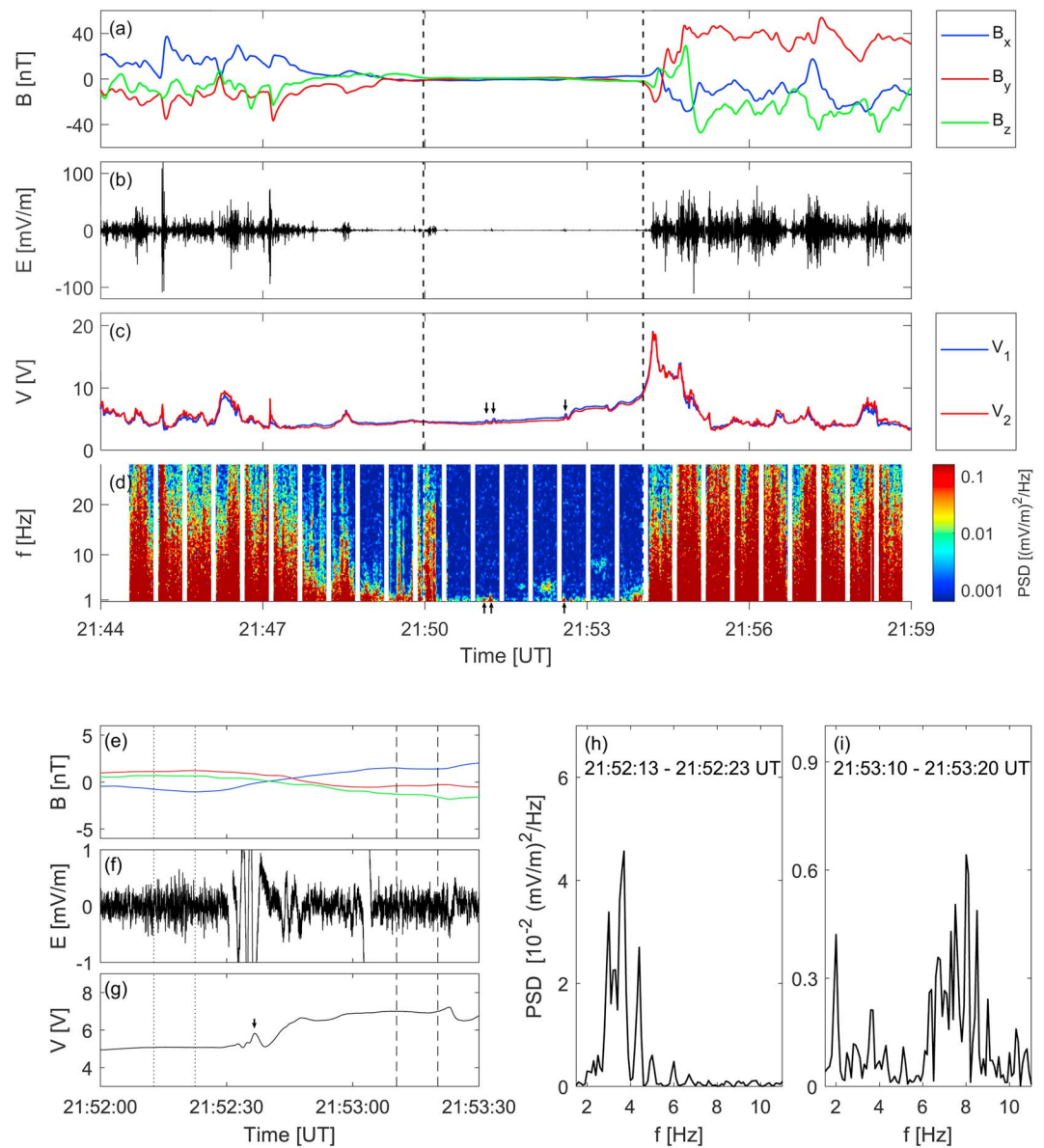


Figure 2. Signatures at crossing B (21:49:59–21:54:03 UT) on 28 May 2015. The same caption as in Figure 1. The black arrows in panels (c) and (d) show the detection of very low frequency electric field signals (about 1 Hz) related to small density peaks. In panels (f) and (g), such a density peak, combined with the presence of a 1-s data gap around 21:52:30 UT, causes great fluctuations in the electric field shortly after the 3.5-Hz signal (corresponding to the third arrow in panels c and d). PSD = power spectral density

time periods encompassing crossings A and B and display PSDs of electric field wave packets related to the activity detected in the spectrograms. Spectra in Figures 1h–i and 2h–i are computed over intervals limited by vertical dashed and dotted lines in panels e–g. In the electric fields inside cavity crossing A (Figure 1f), the increased activity during the gradual temporal evolution of the signal from high (~6 Hz) to low (1–2 Hz) frequencies is detectable by eye. The strong PSD signal close to the transition out of the cavity (panel i) originates from the large-amplitude feature in the electric field (panel f). A qualitatively similar large-amplitude electric field signal is detected around 21:52:30 UT during crossing B (Figure 2f). This coincides with a small density peak (shown by an arrow in Figure 2g), similar to two other signals within the cavity (marked by arrows in Figure 2c–d). However, due to the short signal durations and the data gap coinciding with the 21:52:30 UT signal, these are not further studied here. Figure 2g shows that a sudden increase, albeit small, in the local electron density might be related to the observed increase in PSD frequency from about 3.5 to 7.5 Hz during crossing B. This is, however, not consistent with the behavior of the signals during crossing A, where a small

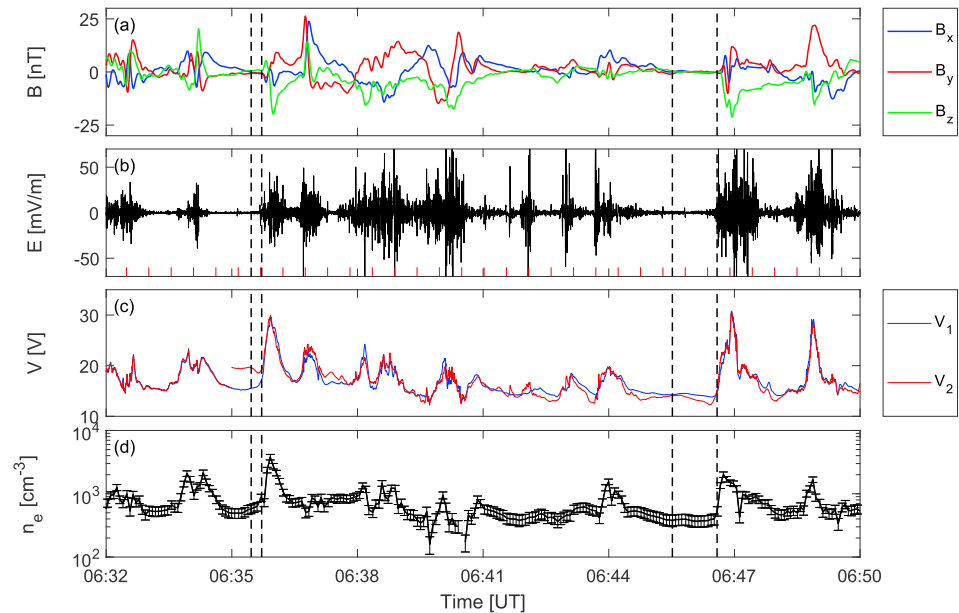


Figure 3. Signatures at crossings C (06:35:29–06:35:44 UT) and D (06:45:32–06:46:36 UT) on 17 February 2016. (a)–(c) The same caption as Figure 1a–1c. The discontinuity in V_2 at 06:35 UT stems from a change in probe calibration due to the partial shadowing of LAP2. The small periodic spikes in the electric field in panel b are caused by the data gaps, marked by vertical red lines. (d) Mutual Impedance Probe-derived electron density, at a temporal resolution varying from 4 to 6 s, with estimated error bars (10–20% on average).

gradual increase in probe potentials coincides with a gradual decrease in detected frequency. For both events, no significant variation in the magnetic field appears related to the sudden electric field activity.

3.2. Electric Field Activity Outside the Diamagnetic Cavity

In the magnetized environment surrounding the cavity, an electric field activity in the same frequency range as inside the cavity is observed. An example is given in Figure 4 for two 10-s time intervals between crossings A and B. We observe similar results for other intervals. During these 10-s intervals, the probe potentials vary, suggesting local plasma density gradients. This coincides with the appearance of wave packets in the electric field (Figure 4c). Fourier PSDs of these are given in Figures 4d and 4e, showing clear peaks at 5.5 and 3.5 Hz, respectively. This is in the range of the theoretical local LH frequency of water ions dominating the inner coma, calculated in Figure 4b as

$$f_{\text{LH}} = \sqrt{\frac{f_{\text{ce}} f_{\text{ci}}}{1 + \frac{f_{\text{ce}}^2}{f_{\text{pe}}^2}}} \approx \sqrt{f_{\text{ce}} f_{\text{ci}}} \quad (1)$$

where f_{ci} and f_{ce} are the ion and electron gyrofrequencies and f_{pe} is the electron plasma frequency (André et al., 2017). During the considered time interval, no MIP electron density could be derived, and the

Table 1

Temporal and Spatial Positions of the Two Cavity Observations on 28 May 2015 (Crossings A and B) and the Two Cavity Crossings on 17 February 2016 (Crossings C and D)

	Date	Time interval (UT)	Extent (s)	$\mathbf{r}_c = (x, y, z)$ (km)	d_c (km)	d_h (AU)
A	15/05/28	21:10:00–21:10:50	50	(110.2, 245.9, –7.0)	269.6	1.54
B		21:49:59–21:54:03	244	(109.7, 244.9, –8.1)	268.5	
C	16/02/17	06:35:29–06:35:44	15	(14.4, –34.1, –20.6)	42.4	2.38
D		06:45:32–06:46:36	64	(14.4, –34.1, –20.5)	42.3	

Note. \mathbf{r}_c is the comet-centered solar equatorial position of the transitions into the cavity, whilst d_c and d_h are the local cometocentric and heliocentric distances, respectively.

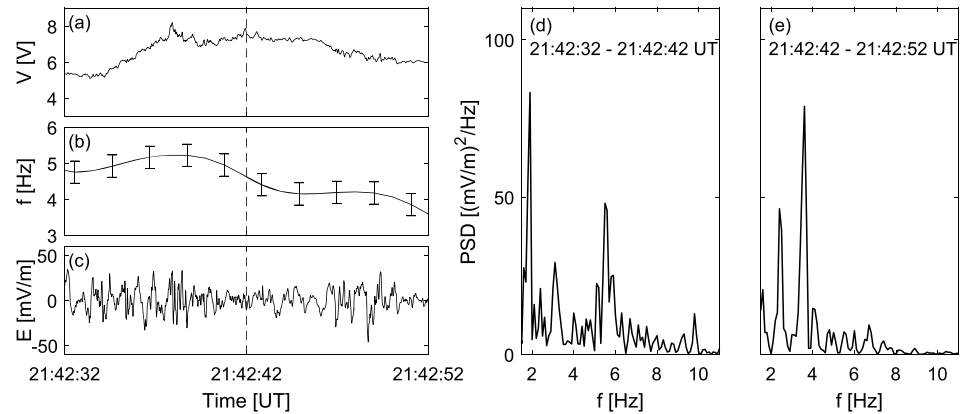


Figure 4. (a)–(c) Averaged probe potential, theoretical lower-hybrid (LH) frequency, and electric field during a 20-s interval occurring between crossings A and B on 28 May 2015. The uncertainty in the LH frequency is computed from the 2-nT uncertainty in the magnetic field calibrated with respect to crossing B. (d)–(e) Electric field power spectral densities (PSDs) during intervals separated by the vertical dashed line in panels a–c.

LAP bias sweep mode was off to allow for electric field measurements. However, a few hours after crossing B, the LAP sweep mode estimated the electron temperature and density to be on the order of 5 eV and 100 cm^{-3} , respectively. Using this and a measured average magnetic field magnitude of $B = 28 \text{ nT}$ gives $f_{ce} \approx 0.78 \text{ kHz}$ and $f_{pe} \approx 90 \text{ kHz}$ such that $f_{ce}^2/f_{pe}^2 \ll 1$, allowing the approximation.

The detection of electric field activity near the water-group LH frequency is consistent with LH wave observations reported by Karlsson et al. (2017) and further discussed by André et al. (2017), in the inner coma of comet 67P. These were attributed to the LHDI related to density gradients, and following the analysis in Karlsson et al. (2017), the three criteria for the LHDI to operate are here considered:

$$L \leq \left(\frac{m_i}{m_e}\right)^{1/4} \rho_{ci}, \quad \beta < \beta_{cr}, \quad \frac{v_{di}}{v_{thi}} > \frac{2f_{ci}}{f_{LH}} \quad (2)$$

Here m_i and m_e are the ion and electron masses, ρ_{ci} is the ion gyroradius, v_{thi} and $v_{di} = \frac{v_{thi}^2}{4\pi f_{ci} L}$ are the ion thermal and diamagnetic drift velocities, $\beta = \frac{n_e k_B (T_e + T_i)}{B^2 / (2\mu_0)}$ with T_i and T_e being the ion and electron temperatures, and $\beta_{cr} \approx 1 - 2$ (Davidson et al., 1977). L is the electron density gradient length scale given by

$$L = \left(\frac{1}{n_e} \frac{dn_e}{dx}\right)^{-1} = -\left(\frac{e}{k_B T_e} \frac{dV_{s/c}}{dx}\right)^{-1} \quad (3)$$

The last equality in equation (3) follows from the orbital-motion-limited theory for a negatively charged spacecraft at potential $V_{s/c}$ in a plasma at constant temperature, assuming that the currents to the spacecraft consists of predominantly electron and a constant photoemission currents (e.g., Odelstad et al., 2015). During the studied events, the spacecraft potential is negative. Therefore, changes in the probe potentials give an estimate of the negative of the spacecraft potential change. Odelstad et al. (2017) showed that the LAP probes only pick up a fraction (between 0.7 and 1) of the spacecraft potential. For an order of magnitude estimate, we assume $\Delta V_{probe} = -\Delta V_{s/c}$. Using this for the two intervals in Figure 4, when the LAP probe potentials change from 5.2 V (at 21:42:32 UT) to 7.8 V (at 21:42:42 UT) and then back to 5.8 V (at 21:42:52 UT), along with the assumption that the plasma gradients are moving across the spacecraft with a speed similar to the speed of the neutrals ($\approx 1 \text{ km/s}$; Hajra et al., 2018; Hansen et al., 2016) give $L = 19\text{--}25 \text{ km} < \left(\frac{m_i}{m_e}\right)^{1/4} \rho_{ci} = 656 \text{ km}$, assuming $T_i = T_e \approx 5 \text{ eV}$. With the same assumption, we get $\beta = 0.5 < \beta_{cr} \approx 1 - 2$, and $\frac{v_{di}}{v_{thi}} = 0.98 - 1.27 > \frac{2f_{ci}}{f_{LH}} = 0.01$. Hence, criteria for the LHDI are fulfilled, suggesting that this instability might excite the detected low-frequency waves outside the cavity in analogy to what was observed by Karlsson et al. (2017) and André et al. (2017) at comet 67P.

4. Discussion and Conclusions

On timescales of the duration of the cavity crossings, the electric field qualitatively follows the behavior of the magnetic field, as expected from the coupling between magnetic and electric fields in a magnetized plasma.

The electric field captures the long inbound boundaries with gradually decreasing fluctuation levels, the cavity with low activity compared to the surrounding magnetized plasma, and the sharp outbound boundaries related to rapid activity increases. In the surrounding plasma, the probe potentials fluctuate noticeably, suggesting local plasma density variations. However, inside the cavity the fluctuation levels drastically decrease, and during all crossings, the sharp outbound transitions are subject to probe potential peaks on the order of 5–15 V. During crossings C and D, a comparison between the sunlit LAP1 potential profile and the MIP-derived electron density (Figures 3c and 3d) suggests that the probe potential boundary peaks were indeed related to increases in the thermal electron density. The similar behavior of the probe potentials during all cavity crossings suggests that the outbound boundary peaks during crossings A and B are also likely caused by electron density increases, in agreement with electron density profiles studied by Nemeth et al. (2016) and Henri et al. (2017) for a number of diamagnetic cavity crossings at 67P. This, along with the similar global cavity features observed in both magnetic and electric fields, asserts that the LAP electric field mode is a reliable tool to image diamagnetic cavity crossings.

The low-frequency electric field signals inside the cavity during crossings A and B are spacecraft-related, related to spacecraft-plasma interactions, or related to the plasma environment of the comet-solar wind interaction region. On the spacecraft, the reaction wheels may interfere with the MAG magnetic field measurements (Glassmeier et al., 2007). During crossings A and B, this interference caused distinct magnetic field signatures in the same frequency range as the detected electric field fluctuations. However, the reaction wheel magnetic field interferences are clear tones that smoothly change in time, whereas the detected electric field signals are rapidly changing in frequency and short-lived. It is therefore deemed unlikely that the reaction wheels are causing the temporally varying signatures observed in the electric field.

As noted, electrostatic waves inside the diamagnetic cavity of 67P have previously been observed in situ by Gunell, Goetz, et al. (2017), who showed examples of IAW inside the cavity, attributing them to the closure of the boundary current. Also, during the Active Magnetospheric Particle Tracer Explorers (Bernhardt et al., 1987; Gurnett et al., 1985; Valenzuela et al., 1986) mission, where barium gas was released in the Earth's magnetosphere and in the solar wind, creating an artificial comet-like diamagnetic cavity, two bands of electrostatic wave emissions below 1 kHz near the barium ion plasma frequency were observed and concluded to be IAW (Gurnett et al., 1985; Gurnett, Anderson, Ma, et al., 1986; Gurnett, Anderson, Bernhardt, et al., 1986). Low-frequency IAW can also be excited by an external forcing on the unmagnetized plasma. For relatively low electron-to-ion temperature ratios, IAW can be damped (McKinstry et al., 1999) and thus observed only close to the forcing region.

The electric field fluctuations observed during crossings A and B are in the same frequency range as low-frequency waves observed in the magnetized plasma surrounding the cavity (Figure 4). These are in the local water-group ion LH frequency range and, as shown in section 3.2, may be driven by the LHDI, similar to the LH waves observed by Karlsson et al. (2017) in the inner coma of comet 67P. LH waves were previously observed in the inner coma of comet 1P/Halley during the Vega 2 flyby (Savin et al., 1986), and waves in the LH frequency range were detected during the Active Magnetospheric Particle Tracer Explorer mission (Bingham et al., 1991). This suggests that inner cometary comae are favorable environments for the generation and growth of LH waves, and hence, the detection of electrostatic activity near the local water-group ion LH frequency in the magnetized plasma close to the contact surface is not unexpected.

LH waves propagate predominantly in the direction perpendicular to the magnetic field, with both the wave and fluctuating electric field vectors orthogonal to the background magnetic field (Parks, 1991; Pécseli, 2012). Thus, they can influence the dynamics of the diamagnetic cavity boundary. It is here suggested that the low-frequency waves detected inside the cavity during crossings A and B are excited by the forcing on the contact surface by the LH waves existing in the magnetized plasma surrounding the cavity. The IAW is the only wave mode in an unmagnetized plasma that matches the frequencies observed by LAP inside the cavity. Hence, we interpret these fluctuations as IAW, excited by the forcing due to the boundary oscillation at the LH frequency. The IAW should be damped far from the boundary by the low-energy electron population detected by instruments aboard the Rosetta spacecraft (Eriksson et al., 2017; Gunell, Goetz, et al., 2017) and are, therefore, expected to subsist only close to the boundary. Furthermore, as indicated by Karlsson et al. (2017), persistent LH activity is related to density gradients. In Figures 1 and 2, the electric field fluctuations inside the cavity are observed close to the boundaries characterized by strong density gradients. The fact that

the signals are observed also within some distance to the boundary, as seen by Rosetta, can be due to the nontrivial topology of the cavity boundary, and Rosetta's trajectory with respect to the boundary.

Standing waves inside a different kind of diamagnetic cavity have been reported in hot flow anomalies in the solar wind near planetary bow shocks (Thomsen et al., 1986; Wang et al., 2013). The wave activity inside these cavities are usually interpreted as being the result of ion-ion beam instabilities arising from intrinsic fluctuations in the solar wind and interaction with the bow shock that acts as a reflecting surface for the incoming plasma (Tjulin et al., 2008). Similarly, in a laboratory study of pressure-gradient-driven instabilities in an argon discharge plasma, Stenzel (1991) reported that IAW could be driven unstable by large electron drifts and temperature gradients, giving rise to turbulence growing in the LH frequency range.

The exact relation between the LH waves observed in the magnetized plasma and the excited low-frequency electrostatic waves (which we identify as IAW) within the diamagnetic cavity needs to be further investigated by kinetic simulations and, possibly, new observations. In particular, answering the question of how long such a wave can be sustained inside the cavity is of importance. Since our measurement within the cavity is essentially along the spacecraft trajectory, one cannot exclude a complex topology of the cavity, and that the observed waves further inside the cavity may in fact be due to a spacecraft trajectory almost tangential to the cavity boundary. Finally, note that the origin and frequencies of IAW discussed here are different from those discussed in Gunell, Goetz, et al. (2017).

The present study demonstrates the existence of extremely low frequency electrostatic waves within the diamagnetic cavity of comet 67P during two crossings. These are interpreted as IAW triggered by oscillations of the cavity boundary at the LH frequency. We have, furthermore, shown that the dual-probe low-frequency electric field mode of the LAP instrument is able to detect the large-scale features of diamagnetic cavities and complements well the magnetic field measurements made by the MAG instrument aboard the Rosetta spacecraft. This supports the reliability of the LAP electric field mode as a tool to further characterize the cometary environment.

Acknowledgments

Rosetta is a European Space Agency (ESA) mission with contributions from its member states and the National Aeronautics and Space Administration (NASA). Work at the University of Oslo was funded by the Research Council of Norway grants 240000 and 230996 and also as part of the 4DSpace Strategic Research Initiative. LAP operations and data handling were supported by the Swedish National Space Board under contract 109/12. Work at the Royal Belgian Institute for Space Aeronomy was supported by the Belgian Science Policy Office through the Solar Terrestrial Centre of Excellence and by PRODEX/ROSETTA/ROSINA PEA4000107705. Work at LPC2E/CNRS was supported by ESEP, by CNES and by ANR under financial agreement ANR-15-CE31-0009-01. The authors acknowledge the ISSI International Team "Plasma Environment of comet 67P after Rosetta" for fruitful discussions. B. M. and C. S. W. thank Arne Pedersen for support and numerous discussions throughout the Master's thesis project and Bjørn Lybekk for maintaining the LAP database at UiO. C. S. W. thanks Sigvald Marholm (UiO) for useful discussions on boundary conditions in PIC simulations. We acknowledge the staff of CDDP and Imperial College London for the use of AMDA and the RPC Quicklook data base (provided by a collaboration between the Centre de Données de la Physique des Plasmas, supported by CNRS, CNES, Observatoire de Paris and Université Paul Sabatier, Toulouse, and Imperial College London, supported by the UK Science and Technology Facilities Council). The Rosetta data will be made available through ESA's Planetary Science Archive (PSA) website. This research has made use of NASA's Astrophysics Data System.

References

- André, M., Odelstad, E., Graham, D. B., Eriksson, A. I., Karlsson, T., Stenberg Wieser, G., & Vigren, E. (2017). Lower hybrid waves at comet 67P/Churyumov-Gerasimenko. *Monthly Notices of the Royal Astronomical Society*, 469, S29–S38. <https://doi.org/10.1093/mnras/stx868>
- Bernhardt, P. A., Rousset-Dupre, R. A., Pongratz, M. B., Haerendel, G., & Valenzuela, A. (1987). Observations and theory of the AMPTE magnetotail barium releases. *Journal of Geophysical Research*, 92, 5777–5794. <https://doi.org/10.1029/JA092iA06p05777>
- Biermann, L., Brosowski, B., & Schmidt, H. U. (1967). The interactions of the solar wind with a comet. *Solar Physics*, 1, 254–284. <https://doi.org/10.1007/BF00150860>
- Bingham, R., Shapiro, V. D., Gil'Man, M., Tsytochik, V. N., & de Angelis, U. (1991). Theory of wave activity occurring in the AMPTE artificial comet. *Physics of Fluids B*, 3, 1728–1738. <https://doi.org/10.1063/1.859984>
- Broiles, T. W., Burch, J. L., Clark, G., Koenders, C., Behar, E., Goldstein, R., et al. (2015). Rosetta observations of solar wind interaction with the comet 67P/Churyumov-Gerasimenko. *Astronomy and Astrophysics*, 583, A21. <https://doi.org/10.1051/0004-6361/201526046>
- Carr, C., Cupido, E., Lee, C. G. Y., Balogh, A., Beek, T., Burch, J. L., et al. (2007). RPC: The Rosetta Plasma Consortium. *Space Science Reviews*, 128, 629–647. <https://doi.org/10.1007/s11214-006-9136-4>
- Cravens, T. E. (1986). The physics of the cometary contact surface. In B. Battrick, E. J. Rolfe, & R. Reinhard (Eds.), *ESLAB Symposium on the Exploration of Halley's Comet* (Vol. 250, pp. 241–246). Axford: ESA Special Publication.
- Cravens, T. E. (1989). Cometary plasma boundaries. *Advances in Space Research*, 9, 293–304. [https://doi.org/10.1016/0273-1177\(89\)90452-3](https://doi.org/10.1016/0273-1177(89)90452-3)
- Cravens, T. E. (1991). Plasma processes in the inner coma. In R. L. Newburn Jr., M. Neugebauer, & J. Rahe (Eds.), *IAU Colloq. 116: Comets in the post-Halley era, Astrophysics and Space Science Library* (Vol. 167, pp. 1211–1255). Dordrecht, Netherlands: Cambridge University Press.
- Davidson, R. C., Gladd, N. T., Wu, C. S., & Huba, J. D. (1977). Effects of finite plasma beta on the lower-hybrid-drift instability. *Physics of Fluids*, 20, 301–310. <https://doi.org/10.1063/1.861867>
- Eriksson, A. I., Boström, R., Gill, R., Åhlén, L., Jansson, S.-E., Wahlund, J.-E., et al. (2007). RPC-LAP: The Rosetta Langmuir Probe instrument. *Space Science Reviews*, 128(1), 729–744. <https://doi.org/10.1007/s11214-006-9003-3>
- Eriksson, A. I., Engelhardt, I. A. D., André, M., Boström, R., Edberg, N. J. T., Johansson, F. L., et al. (2017). Cold and warm electrons at comet 67P/Churyumov-Gerasimenko. *Astronomy and Astrophysics*, 605, A15. <https://doi.org/10.1051/0004-6361/201630159>
- Glassmeier, K.-H. (2017). Interaction of the solar wind with comets: A Rosetta perspective. *Philosophical Transactions of the Royal Society London Ser. A*, 375(20160256), 1–20. <https://doi.org/10.1098/rsta.2016.0256>
- Glassmeier, K.-H., Richter, I., Diedrich, A., Musmann, G., Auster, U., Motschmann, U., et al. (2007). RPC-MAG the fluxgate magnetometer in the Rosetta Plasma Consortium. *Space Science Reviews*, 128(1), 649–670. <https://doi.org/10.1007/s11214-006-9114-x>
- Goetz, C., Koenders, C., Hansen, K. C., Burch, J., Carr, C., Eriksson, A., et al. (2016). Structure and evolution of the diamagnetic cavity at comet 67P/Churyumov-Gerasimenko. *Monthly Notices of the Royal Astronomical Society*, 462, S459–S467. <https://doi.org/10.1093/mnras/stw3148>
- Goetz, C., Koenders, C., Richter, I., Altwegg, K., Burch, J., Carr, C., et al. (2016). First detection of a diamagnetic cavity at comet 67P/Churyumov-Gerasimenko. *Astronomy and Astrophysics*, 588, A24. <https://doi.org/10.1051/0004-6361/201527728>
- Gunell, H., Goetz, C., Eriksson, A., Nilsson, H., Simon Wedlund, C., Henri, P., et al. (2017). Plasma waves confined to the diamagnetic cavity of comet 67P/Churyumov-Gerasimenko. *Monthly Notices of the Royal Astronomical Society*, 469, S84–S92. <https://doi.org/10.1093/mnras/stx1134>

- Gunell, H., Nilsson, H., Hamrin, M., Eriksson, A., Odelstad, E., Maggiolo, R., et al. (2017). Ion acoustic waves at comet 67P/Churyumov-Gerasimenko. Observations and computations. *Astronomy and Astrophysics*, *600*, A3. <https://doi.org/10.1051/0004-6361/201629801>
- Gurnett, D. A., Anderson, R. R., Bernhardt, P. A., Luehr, H., & Haerendel, G. (1986). Plasma waves associated with the first AMPTE magnetotail barium release. *Geophysical Research Letters*, *13*(7), 644–647. <https://doi.org/10.1029/GL013i007p00644>
- Gurnett, D. A., Anderson, R. R., Haeusler, B., Haerendel, G., & Bauer, O. H. (1985). Plasma waves associated with the AMPTE artificial comet. *Geophysical Research Letters*, *12*(12), 851–854. <https://doi.org/10.1029/GL012i012p00851>
- Gurnett, D. A., Anderson, R. R., Ma, T. Z., Haerendel, G., & Paschmann, G. (1986). Waves and electric fields associated with the first AMPTE artificial comet. *Journal of Geophysical Research*, *91*(10), 10,013–10,028. <https://doi.org/10.1029/JA091iA09p10013>
- Hajra, R., Henri, P., Vallières, X., More, J., Gilet, N., Wattiaux, G., et al. (2018). Dynamic unmagnetized plasma in the diamagnetic cavity around comet 67P/Churyumov-Gerasimenko. *Monthly Notices of the Royal Astronomical Society*, *475*(3), 4140–4147. <https://doi.org/10.1093/mnras/sty094>
- Hansen, K. C., Altwegg, K., Berthelier, J.-J., Bieler, A., Biver, N., Bockelée-Morvan, D., et al. (2016). Evolution of water production of 67P/Churyumov-Gerasimenko: An empirical model and a multi-instrument study. *Monthly Notices of the Royal Astronomical Society*, *462*(1), 1–17. <https://doi.org/10.1093/mnras/stw2413>
- Hansen, K. C., Bagdonat, T., Motschmann, U., Alexander, C., Combi, M. R., Cravens, T. E., et al. (2007). The plasma environment of comet 67P/Churyumov-Gerasimenko throughout the Rosetta main mission. *Space Science Reviews*, *128*, 133–166. <https://doi.org/10.1007/s11214-006-9142-6>
- Henri, P., Vallières, X., Hajra, R., Goetz, C., Richter, I., Glassmeier, K.-H., et al. (2017). Diamagnetic region(s): Structure of the unmagnetized plasma around comet 67P/CG. *Monthly Notices of the Royal Astronomical Society*, *469*, S372–S379. <https://doi.org/10.1093/mnras/stx1540>
- Ip, W.-H., & Axford, W. I. (1987). The formation of a magnetic-field-free cavity at Comet Halley. *Nature*, *325*, 418. <https://doi.org/10.1038/325418a0>
- Israelevich, P. L., Ershkovich, A. I., Gombosi, T. I., Neubauer, F. M., & Cohen, O. (2003). Fine structure of the diamagnetic cavity boundary in comet Halley. *Journal of Geophysical Research*, *108*(A2), 1097. <https://doi.org/10.1029/2002JA009622>
- Johansson, F. L., Odelstad, E., Paulsson, J. J. P., Harang, S. S., Eriksson, A. I., Mannel, T., et al. (2017). Rosetta photoelectron emission and solar ultraviolet flux at comet 67P. ArXiv E-prints (Vol. 469, pp. 5626–5635).
- Karlsson, T., Eriksson, A. I., Odelstad, E., André, M., Dickeli, G., Kullen, A., et al. (2017). Rosetta measurements of lower hybrid frequency range electric field oscillations in the plasma environment of comet 67P. *Geophysical Research Letters*, *44*, 1641–1651. <https://doi.org/10.1002/2016GL072419>
- Mandt, K. E., Eriksson, A., Edberg, N. J. T., Koenders, C., Broiles, T., Fuselier, S. A., et al. (2016). RPC observation of the development and evolution of plasma interaction boundaries at 67P/Churyumov-Gerasimenko. *Monthly Notices of the Royal Astronomical Society*, *462*, S9–S22. <https://doi.org/10.1093/mnras/stw1736>
- McKinstrie, C. J., Giacone, R. E., & Startsev, E. A. (1999). Accurate formulas for the Landau damping rates of electrostatic waves. *Physics of Plasmas*, *6*(2), 463–466. <https://doi.org/10.1063/1.873212>
- Meier, P., Glassmeier, K.-H., & Motschmann, U. (2016). Modified ion-Weibel instability as a possible source of wave activity at comet 67P/Churyumov-Gerasimenko. *Annales Geophysicae*, *34*, 691–707. <https://doi.org/10.5194/angeo-34-691-2016>
- Morlet, J., Arens, G., Forgeau, I., & Giard, D. (1982). Wave Propagation and sampling theory. *Geophysical*, *47*, 203–236.
- Nemeth, Z., Burch, J., Goetz, C., Goldstein, R., Henri, P., Koenders, C., et al. (2016). Charged particle signatures of the diamagnetic cavity of comet 67P/Churyumov-Gerasimenko. *Monthly Notices of the Royal Astronomical Society*, *462*, S415–S421. <https://doi.org/10.1093/mnras/stw3028>
- Neubauer, F. M., Glassmeier, K. H., Pohl, M., Raeder, J., Acuna, M. H., Burlaga, L. F., et al. (1986). First results from the Giotto magnetometer experiment at comet Halley. *Nature*, *321*, 352–355. <https://doi.org/10.1038/321352a0>
- Nilsson, H., Wieser, G. S., Behar, E., Gunell, H., Wieser, M., Galand, M., et al. (2017). Evolution of the ion environment of comet 67P during the Rosetta mission as seen by RPC-ICA. *Monthly Notices of the Royal Astronomical Society*, *469*, S252–S261. <https://doi.org/10.1093/mnras/stx1491>
- Odelstad, E., Eriksson, A. I., Edberg, N. J. T., Johansson, F., Vigren, E., André, M., et al. (2015). Evolution of the plasma environment of comet 67P from spacecraft potential measurements by the Rosetta Langmuir probe instrument. *Geophysical Research Letters*, *42*, 10,126–10,134. <https://doi.org/10.1002/2015GL066599>
- Odelstad, E., Stenberg-Wieser, G., Wieser, M., Eriksson, A. I., Nilsson, H., & Johansson, F. L. (2017). Measurements of the electrostatic potential of Rosetta at comet 67P. *Monthly Notices of the Royal Astronomical Society*, *469*(2), S568–S581. <https://doi.org/10.1093/mnras/stx2232>
- Parks, G. K. (1991). *Physics of space plasmas - An introduction*. Redwood City, CA: Addison-Wesley Publishing Co.
- Pécseli, H. L. (2012). *Waves and Oscillations in Plasmas*. Hoboken, NJ: CRC Press.
- Richter, I., Koenders, C., Auster, H.-U., Frühauff, D., Götz, C., Heinisch, P., et al. (2015). Observation of a new type of low-frequency waves at comet 67P/Churyumov-Gerasimenko. *Annales Geophysicae*, *33*, 1031–1036. <https://doi.org/10.5194/angeo-33-1031-2015>
- Savin, S., Avanesova, G., Balikhin, M., Klimov, S., Sokolov, A., Oberc, P., et al. (1986). ELF waves in the plasma regions near the comet. In B. Batrick, E. J. Rolfe, & R. Reinhard (Eds.), *ESLAB symposium on the Exploration of Halley's comet, ESA Special Publication* (Vol. 3, pp. 433–436).
- Simon Wedlund, C., Alho, M., Gronoff, G., Kallio, E., Gunell, H., Nilsson, H., et al. (2017). Hybrid modelling of cometary plasma environments. I. Impact of photoionisation, charge exchange, and electron ionisation on bow shock and cometopause at 67P/Churyumov-Gerasimenko. *Astronomy and Astrophysics*, *604*, A73. <https://doi.org/10.1051/0004-6361/201730514>
- Stenzel, R. L. (1991). Lower-hybrid turbulence in a nonuniform magnetoplasma. *Physics of Fluids B: Plasma Physics*, *3*(9), 2568–2581. <https://doi.org/10.1063/1.859969>
- Thomsen, M. F., Gosling, J. T., Fuselier, S. A., Bame, S. J., & Russell, C. T. (1986). Hot, diamagnetic cavities upstream from the Earth's bow shock. *Journal of Geophysical Research*, *91*(A3), 2961–2973. <https://doi.org/10.1029/JA091iA03p02961>
- Timar, A., Nemeth, Z., Szego, K., Dosa, M., Opitz, A., Madanian, H., et al. (2017). Modelling the size of the very dynamic diamagnetic cavity of comet 67P/Churyumov-Gerasimenko. *Monthly Notices of the Royal Astronomical Society*, *469*(2), S723–S730. <https://doi.org/10.1093/mnras/stx2628>
- Tjulin, A., Lucek, E. A., & Dandouras, I. (2008). Wave activity inside hot flow anomaly cavities. *Journal of Geophysical Research*, *113*, A08113. <https://doi.org/10.1029/2008JA013333>
- Torrence, C., & Compo, G. (1998). A Practical Guide to Wavelet Analysis. *Bulletin of the American Meteorological Society*, *79*, 61–78.
- Trotignon, J. G., Michau, J. L., Lagoutte, D., Chabassière, M., Chalumeau, G., Colin, F., et al. (2007). RPC-MIP: The Mutual Impedance Probe of the Rosetta Plasma Consortium. *Space Science Reviews*, *128*, 713–728. <https://doi.org/10.1007/s11214-006-9005-1>
- Valenzuela, A., Haerendel, G., Foeppl, H., Melzner, F., & Neuss, H. (1986). The AMPTE artificial comet experiments. *Nature*, *320*, 700–703. <https://doi.org/10.1038/320700a0>

- Wang, S., Zong, Q., & Zhang, H. (2013). Hot flow anomaly formation and evolution: Cluster observations. *Journal of Geophysical Research: Space Physics*, *118*, 4360–4380. <https://doi.org/10.1002/jgra.50424>
- Welch, P. D. (1967). The use of fast Fourier transform for the estimation of power spectra: A method based on time averaging over short, modified periodograms. *IEEE Xplore: IEEE Transactions on Audio and Electroacoustics*, *15*, 70–73.